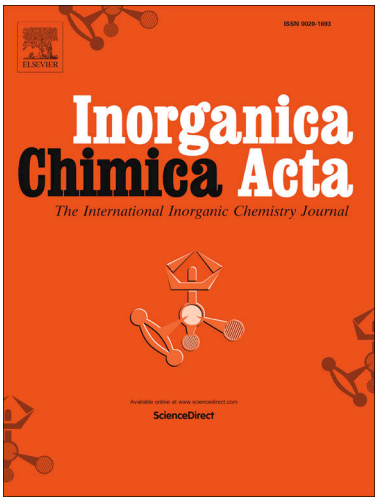

Coordination polymers of *d*- and *f*-elements with (1,4-phenylene)dithiazole dicarboxylic acid

Kostiantyn V. Domasevich, Patrizio Campitelli, Marco Moroni, Simona Bassoli, Giorgio Mercuri, Matteo Pugliesi, Giuliano Giambastiani, Corrado Di Nicola, Andrea Rossin, Simona Galli

PII: S0020-1693(22)00135-9
DOI: https://doi.org/10.1016/j.ica.2022.120923
Reference: ICA 120923

To appear in: *Inorganica Chimica Acta*

Received Date: 1 February 2022
Revised Date: 21 March 2022
Accepted Date: 22 March 2022

Please cite this article as: K.V. Domasevich, P. Campitelli, M. Moroni, S. Bassoli, G. Mercuri, M. Pugliesi, G. Giambastiani, C. Di Nicola, A. Rossin, S. Galli, Coordination polymers of *d*- and *f*-elements with (1,4-phenylene)dithiazole dicarboxylic acid, *Inorganica Chimica Acta* (2022), doi: https://doi.org/10.1016/j.ica.2022.120923

Coordination polymers of *d*- and *f*-elements with (1,4-phenylene)dithiazole dicarboxylic acid

Kostiantyn V. Domasevich,[a] Patrizio Campitelli,[b] Marco Moroni,[c] Simona Bassoli,[c]

Giorgio Mercuri,[d,e] Matteo Pugliesi,[d] Giuliano Giambastiani,[d]

Corrado Di Nicola,[b,] Andrea Rossin[d,]* and Simona Galli[c,]**

[a] Taras Shevchenko National University of Kyiv
Volodymyrska Str. 64/13, 01601 Kyiv, Ukraine.

[b] Scuola di Scienze e Tecnologie, Università di Camerino,
Via S. Agostino 1, 62032 Camerino, Italy.

[c] Dipartimento di Scienza e Alta Tecnologia, Università dell'Insubria,
Via Valleggio 11, 22100 Como, Italy.

[d] Istituto di Chimica dei Composti Organometallici (ICCOM-CNR),
Via Madonna del Piano 10, 50019 Sesto Fiorentino, Italy.

[e] Scuola del Farmaco e dei Prodotti della Salute, Università di Camerino,
Via S. Agostino 1, 62032 Camerino, Italy.

Authors to whom correspondence should be addressed:

Prof. Simona Galli (simona.galli@uninsubria.it);

Dr. Corrado Di Nicola (corrado.dinicola@unicam.it);

Dr. Andrea Rossin (a.rossin@iccom.cnr.it).

Abstract

The new ditopic ligand [2,2'-(1,4-phenylene)bithiazole]-5,5'-dicarboxylic acid (**H_2TzPhTz**) was synthesized in ~70% yield through a classical Hantzsch synthesis. Isolation of the dimethyl ester intermediate **Me_2TzPhTz** as the trifluoroacetic acid adduct **Me_2TzPhTz·2CF_3CO_2H** allowed its crystal structure determination, revealing that the constituting molecules are interconnected through an extended hydrogen-bond network. Reaction of **H_2TzPhTz** with suitable Zn^{II} and U^{VI} salts yielded the 1-D coordination polymers [Zn(TzPhTz)(H_2O)$_2$] (**Zn_TzPhTz**) and [UO_2(TzPhTz)(DMF)]·DMF (**U_TzPhTz**). The former is characterized by zig-zag chains with *cis*-{Zn(O_{COO})$_4$(O_{H2O})$_2$} nodes and μ-η^2:η^2-**TzPhTz**$^{2-}$ spacers, while in the latter **TzPhTz**-bridged {UO_2(TzPhTz)(DMF)}$_2$ dimeric units form polymeric strands. In the solid state, both **H_2TzPhTz** and **Zn_TzPhTz** emit in the blue-green visible region (λ_{em} = 474 and 477 nm, respectively). The two coordination polymers witness the versatility of **H_2TzPhTz** as a linker toward *d* and *f* metal ions, and they should be considered as the preliminary step toward the preparation of **TzPhTz**-based metal-organic frameworks for practical applications in the field of luminescence sensing.

Keywords

Coordination Polymers, Zinc, Uranium, Thiazole, Powder X-ray Diffraction (PXRD), Single-crystal X-ray Diffraction, UV-Vis spectroscopy

Highlights

- [2,2'-(1,4-phenylene)bithiazole]-5,5'-dicarboxylic acid (H_2TzPhTz) has been prepared for the first time *via* the classical Hantzsch synthesis
- [Zn(TzPhTz)(H_2O)$_2$] shows hydrogen-bonded 1-D zig-zag chains with *cis*-{Zn(O_{COO})$_4$(O_{H2O})$_2$} nodes and μ-η^2:η^2-TzPhTz spacers
- [UO_2(TzPhTz)] features {UO_2(TzPhTz)(DMF)}$_2$ dimeric units along 1-D strands
- H_2TzPhTz and [Zn(TzPhTz)(H_2O)$_2$] emit in the blue-green visible region

1. Introduction

The world of coordination polymers (CPs) and metal-organic frameworks (MOFs) has been steadily expanding in the past 25 years [1]. As a representative proof, more than 100,000 crystal structures of MOFs [2] have been deposited in the Cambridge Structural Database up to 2021, and their number is growing daily. This growth is mainly due to the vast library of metal nodes and organic linkers and to their versatility in assembling, which allows for the tailor-made design and preparation of compounds suitable for target applications. [1b, 3]

The scientific literature proposes countless examples of linkers with N-containing heterocycles [4] successfully employed in the preparation of CPs and MOFs [5]. As representative members of this family, we quote imidazoles [6], pyrazoles [7], triazoles [8], and tetrazoles [9].

At variance, much fewer cases of linkers with S-containing heterocycles have been reported for the same purpose [10]. Interesting examples in this respect are present with tetrathiafulvalenes [11].

Thiazoles are the simplest and most naturally occurring (N,S)-containing heterocycles [4]. The simultaneous presence of two heteroatoms with a pronounced difference in their Lewis basicity, like nitrogen (a hard base) and sulphur (a soft base), causes a modification of the ring electron density distribution if compared with purely N- or purely S-containing heteroaromatic rings.

The preparation of MOFs and CPs containing thiazoles as constituting part of the organic linker has been the main research focus of some of us in the past ten years [12]. Recently, we have reported the synthesis and characterization of a new dicarboxylic acid with a conjugated bithiazole core, namely: [2,2'-bithiazole]-5,5'-dicarboxylic acid (H_2TzTz, Scheme 1) [13]. The presence, in this linker, of medium-strength basic sites (the thiazole N atoms, pK_a = 2.5 [14]) potentially improves the interactions of the MOF pore walls with acidic guests like carbon dioxide. Indeed, in combination with Zr^{IV}, H_2TzTz yielded the UiO-67 analogue [$Zr_6O_4(OH)_4$(TzTz)$_6$], successfully exploited [13] in carbon capture and conversion and in CO_2 storage and utilization to prepare cyclic carbonates. In addition, H_2TzTz is luminescent, emitting in the blue-visible region upon suitable excitation with an UV source. The luminescent properties in a series of Zr^{IV} (MIX)MOFs with UiO-67 topology and containing H_2TzTz have been recently studied

[15]. Based on these premises, we have planned to prepare the longer analogue of H_2TzTz through the insertion of a phenyl core between the thiazole rings, this yielding the [2,2'-(1,4-phenylene)bithiazole]-5,5'-dicarboxylic acid (**H_2TzPhTz**, Scheme 1). This newly synthesized ligand has been thoroughly characterized in solution (^{1}H and ^{13}C NMR spectroscopy) and in the solid state (elemental analysis, IR spectroscopy, thermogravimetric analysis, differential thermal analysis). Subsequently, we have tested its coordination ability toward *d* and *f* metal ions, isolating the two coordination polymers [Zn(TzPhTz)(H_2O)$_2$] (**Zn_TzPhTz**) and [UO_2(TzPhTz)(DMF)]·DMF (**U_TzPhTz**), which we have characterized in the solid state. These preliminary results open promising horizons in the synthesis of **H_2TzPhTz**-containing luminescent MOFs featured by high specific surface area exploitable for luminescence sensing.

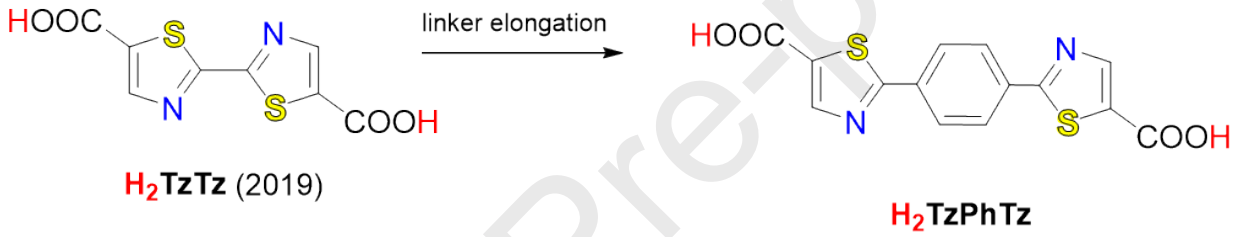

H_2TzTz (2019) **H_2TzPhTz**

Scheme 1. Molecular structures of [2,2'-bithiazole]-5,5'-dicarboxylic acid (H_2TzTz) and [2,2'-(1,4-phenylene)bithiazole]-5,5'-carboxylic acid (**H_2TzPhTz**).

2. Experimental Section

2.1. Materials and Methods. Commercially available reagents were purchased from vendors and used as received, without further purification. Commercially available solvents used in the organic syntheses were purchased from vendors and were purified by standard distillation techniques before use. Deuterated solvents were stored over 4 Å molecular sieves and degassed by three freeze-pump-thaw cycles before use. The room temperature ^{1}H NMR spectra of **H_2TzPhTz** and **Me_2TzPhTz** were recorded in DMSO-d_6 at 500 or 400 MHz with a Bruker Ascend 500 or a Bruker AVANCE 400 instrument, respectively. The room temperature ^{13}C NMR spectrum of **H_2TzPhTz** was recorded in DMSO-d_6 at 125 MHz with a Bruker Ascend 500 instrument. In the following, the ^{1}H and ^{13}C{^{1}H} chemical shifts, calibrated against the

resonance of the residual hydrogen atoms of the deuterated solvent, are reported in parts per million (ppm) downfield of tetramethylsilane (TMS). The IR spectra of the **H_2TzPhTz** ligand and the **Zn_TzPhTz** coordination polymer were recorded as neat from 4000 to 600 cm^{-1} with a PerkinElmer Spectrum One System instrument. Elemental analyses (mass percentages of C, H, N, S) were performed with a Fisons Instruments 1108 CHNS-O elemental analyzer. Thermogravimetric analyses and differential thermal analyses of the **H_2TzPhTz** ligand and the **Zn_TzPhTz** coordination polymer were performed with a Perkin Pyris 1 thermal analyser heating from 303 to 873 K with a speed of 10 K/min, under a 25 mL/min nitrogen flux. UV-Vis absorption diffuse reflectance spectra of **H_2TzPhTz** and **Zn_TzPhTz** in the solid state were recorded from 250 to 600 nm with a Jasco V-770 spectrophotometer equipped with a 60 mm integrating sphere and a PbS detector (ISN-923), using an interval wavelength of 1 nm,. Fluorescence spectra of **H_2TzPhTz** and **Zn_TzPhTz** in the solid state were recorded with a JascoFP-8300 spectrofluorometer equipped with a 150 W Xenon arc lamp. The samples were irradiated at the wavelength corresponding to their maximum absorption, as revealed by the absorption spectrum.

2.2. Ligand synthesis. The multi-step procedure adopted in this work to prepare the **H_2TzPhTz** ligand starting from 1,4-dicyanobenzene (terephthalonitrile) is summarized in Scheme 2. All the stages of this synthesis are easily scalable and take advantage of cheap reagents under accessible reaction conditions.

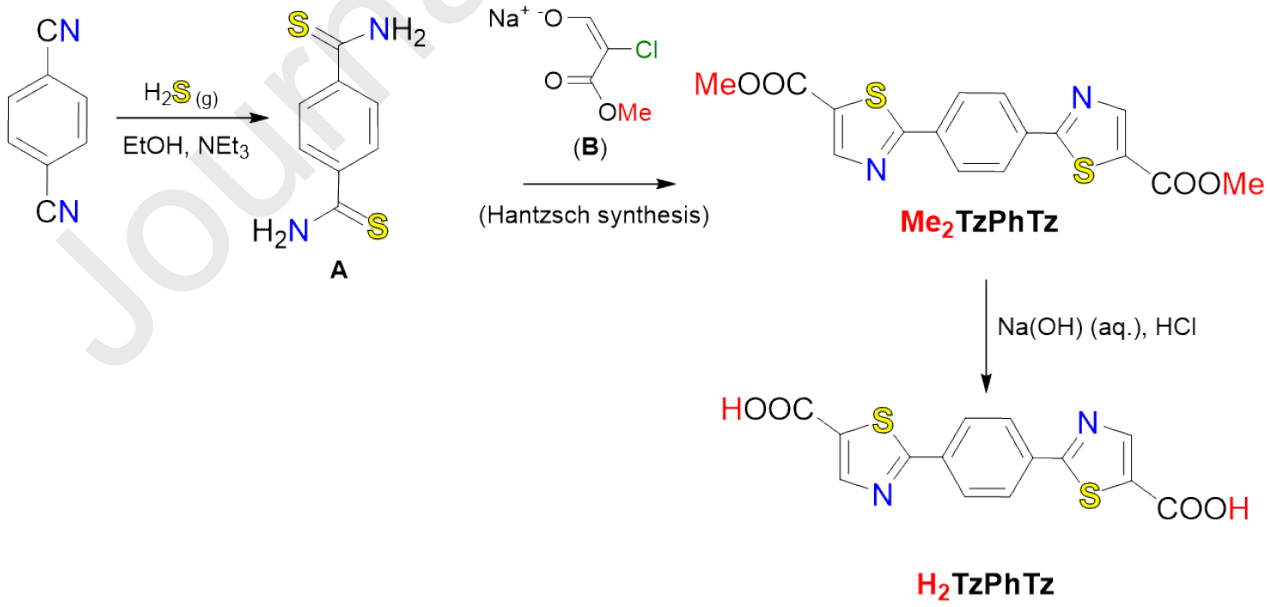

Scheme 2. Preparation of **H_2TzPhTz**.

2.2.1. Synthesis of benzene-1,4-dithiocarboxamide (A). The proposed method is superior to the known literature preparations of benzene-1,4-dithiocarboxamide, commonly utilizing exceedingly large volumes of dry pyridine as solvent [16]. Terephthalonitrile (Scheme 2) (16.0 g, 0.13 mol) was suspended in a mixture of 95% v/v ethanol (400 mL) and triethylamine (80 mL). A slow to medium stream of hydrogen sulphide, produced as detailed in section S1 of the Electronic Supplementary Information (ESI), was bubbled through the reaction mixture, which was kept under magnetic stirring for 4 h. The colourless solution slowly turned to orange in 1 h. Most of terephthalonitrile was dissolved after 1.5 h, while the temperature of the system gradually raised to 305-307 K. The reaction product deposited as a fine yellow powder. The H_2S bubbler was removed and the mixture was stirred for additional 5 h. Then, it was left still overnight. The yellow solid was filtered and washed with 95% v/v ethanol (50 mL) and dichloromethane (100 mL). To the orange reaction filtrate, terephthalonitrile (8.0 g, 0.06 mol) was further added and hydrogen sulphide was bubbled for 2.5 h under magnetic stirring. The mixture was stirred for additional 5 h, then it was left still overnight. Finally, it was filtered, and the yellow precipitate was washed with 95% v/v ethanol (50 mL) and dichloromethane (100 mL). The two portions of benzene-1,4-dithiocarboxamide (**A**, Scheme 2) thus obtained were combined and dried for 2 d in air. Yield: 35.8 g (97%). m.p. = 272-273 ^{o}C (dec.) *vs*. yield: 99% and m.p. = 269-273 ^{o}C (dec.) [16a]; yield 93% and m.p. = 257-258 ^{o}C [16b]. The ^{1}H NMR and IR spectra of our samples agree with those reported in the literature [16b].

2.2.2. Synthesis of the sodium enolate of methyl formylchloroacetate (B). Bulk sodium (21.3 g, 0.93 mol) was cut into pieces of 2-3 mm size with a Swiss knife under xylene and subsequently transferred into a 2 L flask containing dry benzene (700 mL). Methanol (5.0 mL, 0.12 mol) was added, and the mixture was stirred for 1 h at ambient temperature. When the evolution of hydrogen ceased, the flask was placed into a cooling bath and the mixture was cooled to 278 K. Then, methyl formate (10.0 mL, 0.16 mol) was added in one portion. A mixture of methyl formate (68.3 mL, for a total of 1.27 mol including the above 10.0 mL portion) and methyl chloroacetate (85.2 mL, 0.97 mol) was added dropwise at 277-278 K, during a 3 h period and under vigorous magnetic stirring. A small quantity of heat evolved from

the reaction. The reaction progress was monitored through the complete dissolution of sodium and the deposition of a fine colourless powder. After the addition of methyl formate and methyl chloroacetate was complete, the mixture was stirred for additional 5-6 h at 278-280 K to complete the dissolution of sodium, then it was left still overnight in a cooling bath. The resulting mixture was composed by a yellow solution and a significant amount of light-cream coloured precipitate of the sodium enolate of methyl formylchloroacetate (**B**, Scheme 2). The precipitate was filtered, it was thoroughly washed with benzene (200 mL) and it was dried in air for several hours. Yield: 117.6 g [contaminated with 21.5% m/m of NaCl. The purity of the sample was estimated as 78.5% based on a titration with $HCl_{(aq)}$]. When reacted with thiourea in aqueous solution, formylchloroacetate gives the known 2-amino-5-carbomethoxythiazole in 71% yield, m.p. = 188-190 °C [34]. The sodium enolate of methyl formylchloroacetate is not hygroscopic, but it is only moderately stable: it turns yellow and then it darkens after several days at room temperature, but it may be stored for a longer period in a freezer.

2.2.3. Hantzsch synthesis of dimethyl [2,2'-(1,4-phenylene)bithiazole]-5,5'-carboxylate (Me_2TzPhTz). Solid benzene-1,4-dithiocarboxamide **A** (24.11 g, 0.12 mol) was added in one portion under magnetic stirring to a dimethylformamide (DMF) solution (500 mL) of the sodium enolate of methyl formylchloroacetate **B** (99.35 g, 78.5% purity as above; 0.49 mol). The flask was immersed into a glycerol bath pre-heated to 328-330 K and the mixture was stirred at this temperature for 24 h. Within 3-4 h, the solution turned from bright yellow to red-brown, and an almost colourless precipitate was formed. After 24 h, the mixture was cooled and filtered. The solid was thoroughly washed with DMF (70 mL) and methanol (70 mL). Then it was transferred into a beaker and stirred with water (400 mL) to dissolve the excess sodium chloride. The remaining brown powder of **Me_2TzPhTz** was filtered, repeatedly washed with water (70 mL *per* portion) and finally with methanol (70 mL). Yield: 31.30 g (71%). **Me_2TzPhTz** is insoluble in water, alcohols, cold DMF; it is slightly soluble in boiling chloroform, and it is soluble in boiling DMF, dimethylsulfoxide, 1,2-dichlorobenzene, and trifluoroacetic acid (CF_3CO_2H). Pure **Me_2TzPhTz** was obtained after recrystallization from DMF (7.5 g *per* 1 L). **Me_2TzPhTz** sublimes above 553 K, forming yellow needles, and melts at 580 K (Figure S1). IR (cm^{-1},

Figure 1): 3094 (w) ν(C-H_{arom}), 2960 (w) ν(C-H_{CH3}), 1715 (vs) ν(C=O), 1507 (s), 1437 (s), 1392 (s), 1323 (s), 1290 (s), 1197 (m), 1154 (s), 1093 (s), 981 (m), 948 (m), 895 (m), 837 (s), 795 (m), 770 (m), 751 (m), 636 (s), 452 (m). ^{1}H-NMR (DMSO-d_6, 400 MHz, 298 K): δ (ppm) = 8.55 (s, 2H, C$H_{thiazole}$), 8.07 (m, 4H, C$H_{benzene}$), 3.87 (s, 6H, CH_3). The ^{13}C NMR spectrum could not be recorded due to the extremely low solubility of the compound in DMSO (even at temperatures higher than ambient).

2.2.4. Hydrolysis of dimethyl [2,2'-(1,4-phenylene)bithiazole]-5,5'-dicarboxylate (Me_2TzPhTz) to [2,2'-(1,4-phenylene)bithiazole]-5,5'-dicarboxylic acid (H_2TzPhTz). Me_2TzPhTz (18.00 g, 0.05 mol) was suspended in aqueous NaOH (130 g, 3.25 mol in 1.5 L of warm water). The mixture was refluxed for 8 h under vigorous magnetic stirring. The fine bright yellow powders of the sodium salt were filtered and, without washing, they were collected and dissolved in warm water (3 L at 323-333 K). A very small amount of insoluble material was filtered off. Then, the clear yellowish solution was acidified by dropwise addition of aqueous HCl 3.5% m/m (250 mL; final value of pH = 4) under vigorous magnetic stirring. The precipitate of **H_2TzPhTz** (Scheme 2) was stirred in solution for additional 3-4 h at 323-333 K, then it was filtered off, it was repeatedly washed with water, methanol, and diethyl ether, and it was dried for 5 h at 353-363 K giving a light-yellow powder. Yield: 15.92 g (96%). Elem. anal. (%): calcd. for $C_{14}H_8N_2O_4S_2$ (MW = 332.35 a.m.u.): C, 50.60; H, 2.43; N, 8.43; S, 19.29. Found: C, 50.24; H, 2.43; N, 8.35; S, 19.72. IR (cm^{-1}; Figure S1 of the ESI): 3092 (w) and 2989 (m) ν(C-H_{arom}), 2853 (m), 2686 (m), 2540 (m), 1653 (s) ν(C=O), 1526 (m), 1506 (s), 1433 (s), 1417 (s), 1390 (m), 1292 (s), 1251 (s), 1155 (s), 1100 (s), 1029 (w), 983 (m), 897 (s), 834 (s), 778 (m), 758 (s), 666 (m), 635 (s). ^{1}H-NMR (DMSO-d_6, 500 MHz, 298 K): δ (ppm) = 8.47 (s, 2H, C$H_{thiazole}$), 8.16 (s, 4H, C$H_{benzene}$). ^{13}C-NMR (DMSO-d_6, 125 MHz, 298 K): δ (ppm) = 171.08 (s, S-*C*-$N_{thiazole}$), 162.42 (s, O-*C*-$OH_{carbonyl}$), 149.43 (s, *C*-$N_{thiazole}$), 134.97 (s, C_{phenyl}), 131.56 (s, *C*-$S_{thiazole}$), 127.99 (s, *C*H_{phenyl}). TGA/DTA (Figure S2 of the ESI): decomposition at 513 K leaving a black residue corresponding to about 7% of the initial weight.

2.3. Synthesis of 1,4-di(5-carbomethoxythiazol-2-yl)benzene trifluroacetic acid 1:2 cocrystal (Me_2TzPhTz·2CF_3CO_2H). This molecular adduct was prepared by slow evaporation of a solution of **Me_2TzPhTz** (100 mg, 0.3 mmol) in CF_3CO_2H (3 mL) at ambient conditions. **Me_2TzPhTz**·2CF_3CO_2H

crystallizes as large colourless plates suitable for single-crystal X-ray diffraction. The compound is unstable in air, readily losing CF_3CO_2H within few minutes with concomitant loss of crystallinity, but it may be stored in the mother liquors.

2.4. Synthesis of [Zn(TzPhTz)(H_2O)$_2$] (Zn_TzPhTz). The reaction was performed under solvothermal conditions by adding zinc(II) acetate dihydrate [$Zn(CH_3COO)_2 \cdot 2H_2O$, 0.110 g, 0.5 mmol] to a DMF solution (10 mL) of **H_2TzPhTz** (0.166 g, 0.5 mmol). The reaction mixture was kept under magnetic stirring at 393 K for 48 h and it was subsequently slowly cooled (4 K/h) to room temperature. A pale-yellow precipitate of **Zn_TzPhTz** was obtained, filtered off, washed twice with DMF and dried under vacuum. Yield: 138 mg (64%). The solid is not soluble in common solvents (water, alcohols, acetonitrile, acetone, ethers, chlorinated solvents, DMF, dimethylsulfoxide). Elem. anal. (%): calcd. for $C_{14}H_{10}N_2O_6S_2Zn$ (MW = 431.74 a.m.u.): C, 38.95; H, 2.33; N, 6.49; S, 14.85. Found: C, 39.20; H, 2.52; N, 6.76; S, 14.88. IR (cm^{-1}; Figure 2): 3095 (w) and 2989 (w) ν(C-H_{arom}), 1560 (s) ν(C=O), 1523 (m), 1511 (m), 1427 (s), 1404 (s), 1385 (s), 1310 (w), 1248 (w), 1160 (m), 1113 (w), 988 (m), 918 (w), 831 (m), 781 (m).

2.5. Synthesis of [UO_2(TzPhTz)(DMF)]·DMF (U_TzPhTz). The reaction was performed in solvothermal conditions reacting uranium(VI) nitrate oxide dihydrate [$UO_2(NO_3)_2 \cdot 2H_2O$, 21.5 mg, 0.05 mmol] and **H_2TzPhTz** (20.0 mg, 0.06 mmol) in DMF (4 mL). The mixture was sealed in a 20 mL Teflon-lined autoclave. The latter was heated to 413 K and it was left at this temperature for 24 h. Then, it was cooled to ambient temperature along 48 h. Small bright-yellow prismatic crystals of **U_TzPhTz** suitable for single-crystal X-ray diffraction were formed in low yield, in a mixture with a dark unidentified material.

2.6. Powder X-ray diffraction structure determination of Zn_TzPhTz. The powder X-ray diffraction patterns were collected at room temperature using a Bruker AXS D8 Advance θ:θ geometry diffractometer, provided with a sealed X-ray source (Cu Kα, λ = 1.5418 Å), a Bruker Lynxeye linear position-sensitive detector, a filter of nickel in the diffracted beam and the following optical components:

Soller slits on the primary and secondary beam (aperture: 2.5°), fixed divergence slit (aperture: 0.5°), anti-scatter slit (aperture: 8 mm). The generator was set at 40 kV and 40 mA. A preliminary PXRD acquisition was carried out in the 2θ range 3.0-35.0°, with steps of 0.02° and a time *per* step of 1 s to assess the purity and crystallinity of the sample. A second PXRD acquisition was carried out in the 2θ range 5.0-105.0°, with steps of 0.02° and a time *per* step of 10 s to solve the crystal and molecular structure. In both cases, a sample (*ca*. 50 mg) of **Zn_TzPhTz** was deposed on a silicon free-background sample-holder 0.2 mm deep (Assing S.r.l., Monterotondo, Italy). The Singular Value Decomposition approach [17], implemented in the software TOPAS-R v.3 [18], was employed to identify sensible space group and unit cell parameters. Subsequently, a whole powder pattern refinement with the so-called Le Bail method [19] was performed with TOPAS-R v.3 to optimize instrument- and sample-dependent variables which were kept fixed during the next step. To solve the crystal structure, the metal centre was treated as a single atom, while the ligand and the water molecules were described as rigid groups. In the case of the ligand, bond distances and angles were assigned after a search in the Cambridge Structural Database [20] for room-temperature crystal structures containing thiazole-based organic molecules [21]. The structure determination was performed using the Simulated Annealing approach [22] implemented in TOPAS-R v.3, varying *i*) the fractional coordinates of the metal centre as well as of the centre of mass of the rigid groups, *ii*) the orientation of the rigid groups. A Chebyshev-type polynomial function was employed to describe the background. The peak profile was modelled trough the Fundamental Parameters Approach [23]. An isotropic thermal factor [$B_{iso}(M)$] was refined for the Zn^{II} ion; the isotropic thermal factor of the atoms belonging to the ligand and the water molecules was calculated as $B_{iso}(L) = B_{iso}(M) + 2.0$ (Å^2). The anisotropic peak broadening was described by means of Gaussian spherical harmonics. The preferred orientation was modelled along the [1 0 -2] pole using the approach of March and Dollase [24]. Finally, the crystal structure was refined with the so-called Rietveld method [25] working in the 2θ range 9.0-105.0° and refining all the variables held fixed during the structure determination step. The final Rietveld refinement plot is shown in Figure S2 of the ESI. The graphical representations of the crystal structure were made using the program Diamond 2.1e [26].

Crystallographic data for [Zn(TzPhTz)(H_2O)$_2$]: $C_{14}H_{10}N_2O_6S_2Zn$, FW = 431.8 a.m.u., monoclinic, *Pc*, a = 8.6677(2) Å, b = 5.5423(1) Å, c = 16.6381(4) Å, β = 105.854(1)°, V = 768.86(3) Å^3, $Z = Z' = 2$, ρ = 1.865 g cm^{-3}, $F(000) = 436$, $R_{Bragg} = 2.81\%$, $R_p = 4.01\%$ and $R_{wp} = 5.45\%$, for 4801 data and 78 parameters, refined in the range 9.0-105.0° (2θ). CCDC no. 2144493.

2.6. Single-crystal X-ray diffraction structure determination of Me_2TzPhTz·2CF_3CO_2H and U_TzPhTz. Single-crystal X-ray diffraction data of **Me_2TzPhTz·2CF_3CO_2H** and **U_TzPhTz** were collected at 213 K with graphite-monochromated Mo Kα radiation (λ = 0.71073 Å) using a Stoe Image Plate Diffraction System. A face-indexed numerical absorption correction was performed using X-RED [27] and X-SHAPE [28]. The data of **Me_2TzPhTz**·2CF_3CO_2H were integrated with a soft overlap tolerance at 8 pixels. The crystal structures were solved by direct methods and refined by full-matrix least-squares on F^2 using the programs SHELXS-97 [29] and SHELXL-2014/7 [30], respectively. All non-hydrogen atoms were refined anisotropically. For **Me_2TzPhTz·2CF_3CO_2H**, all hydrogen atoms were located in difference Fourier maps and refined isotropically, applying similarity restraints to the methyl C-H bond lengths. In the case of **U_TzPhTz**, the hydrogen atoms were positioned geometrically and then refined as riding, with $U_{iso}(H) = 1.5U_{eq}(C_{methyl})$ and $1.2U_{eq}(C_H)$. In the case of **U_TzPhTz**, the high values of the atomic displacement parameters of the solvent molecule indicated potential disorder. Nonetheless, we were unable to model it with partial contributions from different orientations of the solvent molecule. The graphical representations of the crystal structures were made using the program Diamond 2.1e [26].

Crystallographic data for **Me_2TzPhTz·2CF_3CO_2H**: $C_{20}H_{14}F_6N_2O_8S_2$, FW = 588.45 a.m.u., monoclinic, $P2_1/n$, a = 7.1370(3) Å, b = 30.0152(18) Å, c = 10.9860(5) Å, β = 97.749(5)°, V = 2341.6(2) Å^3, $Z = Z' = 4$, ρ = 1.669 g cm^{-3}, $F(000)$ = 1192, θ_{min} = 2.71°, θ_{max} = 27.87°, measured reflections = 20358, independent reflections = 5192, observed [$I > 2\sigma(I)$] reflections = 3336, parameters = 399, restraints = 18, $R1$ [$I > 2\sigma(I)$] = 3.8%, $wR2$ (all data) = 9.6%, GoF = 0.88. CCDC no. 2144491.

Crystallographic data for [UO_2(TzPhTz)(DMF)]·DMF: $C_{20}H_{20}N_4O_8S_2U$, FW = 1493.10 a.m.u., triclinic, *P*-1, a = 9.3571(4) Å, b = 10.8284(5) Å, c = 13.1342(5) Å, α = 76.444(5)°, β = 77.899(5)°, γ =

73.479(5)°, V = 1225.62(10) Å^3, $Z = Z' = 2$, ρ = 2.023 g cm^{-3}, $F(000)$ = 713, θ_{min} = 3.00°, θ_{max} = 27.87°, measured reflections = 13018, independent reflections = 5406, observed [$I > 2\sigma(I)$] reflections = 4296, parameters = 320, restraints = 0, $R1$ [$I > 2\sigma(I)$] = 2.4%, $wR2$ (all data) = 4.9%, GoF = 0.83. CCDC no. 2144492.

3. Results and Discussion

3.1. H_2TzPhTz: synthesis. To prepare **H_2TzPhTz** we exploited the Hantzsch synthesis, *i.e.* the condensation between an α-halocarbonyl compound and a thioamide [31]. Several published procedures were considered, and they were essentially improved and adapted for large scale and cost-effective preparations. More in detail, common literature preparations of benzene-1,4-dithiocarboxamide (**A**, Scheme 2) are unsuitable because of the use of large volumes of pyridine as solvent (*ca*. 400 mL *per* 10 g of substrate) that cannot be recovered [32]. The kinetic data for the thio-hydrolysis of aromatic nitriles [33] suggest higher reaction rates in ethanol, with a much greener synthetic protocol. Moreover, after the separation of the insoluble reaction product **A**, the filtrate (already saturated with hydrogen sulphide) may be directly used to prepare a new batch of **A**.

The key stage (the Hantzsch synthesis) was performed using the sodium enolate of methyl formylchloroacetate (**B**, Scheme 2) as the α-halocarbonyl compound. **B** was freshly prepared by implementing a slight modification to a standard procedure [33], reacting methyl formate, methyl chloroacetate and sodium in the presence of a small amount of methanol in benzene. The preparation of the *methyl* ester (**Me_2TzPhTz**, Scheme 2) is essential, as suggested by Faith [34], since the reaction product is deposited in the form of a fine powder and no difficulties are associated with stirring the reaction mixture. In the case of the (more common) preparation of *ethyl* esters, the reaction mixture becomes jelly even under significant dilution (up to four times more diluted than in the present case), precluding any efficient stirring. The utilization of the sodium enolate **B** for the Hantzsch synthesis is crucial, since it avoids the isolation and handling of the unstable formylchloroacetate. The reaction between **A** and **B** was not successful in either ethanol, water or aqueous dioxane under reflux, due to the

insolubility of **A** and the fast decomposition of **B**. Therefore, the synthesis was performed in DMF, where **A** is sufficiently soluble. The optimized protocol involves stirring the reaction mixture at 328-333 K for 24 h. The addition of acid, to liberate methyl formylchloroacetate from the sodium enolate, was not required. Before performing the hydrolysis of **Me_2TzPhTz** to the corresponding dicarboxylic acid, the dimethyl ester was thoroughly purified through two successive recrystallizations from DMF. The hydrolysis proceeds smoothly in $NaOH_{(aq)}$ 5-7% m/m under reflux. The sodium dicarboxylate salt thus formed is insoluble in the reaction medium and it deposits as a fine bright-yellow powder. This material is relatively soluble in water (without excess of NaOH). Thus, after completion of the hydrolysis the product was filtered from a strongly alkaline solution, and it was dissolved in water (about 7 g *per* 1 L). Any undissolved material was removed by filtration. The insoluble diacid **H_2TzPhTz** was then precipitated by slow addition of an aqueous solution of HCl. In the solid-state FT-IR spectrum of **H_2TzPhTz** (Figure 1), the weak bands in the range 3000-3200 cm^{-1} can be assigned to the ν(C–H) stretching vibration of aromatic hydrogen atoms, whereas the very broad signal between 2900 and 2200 cm^{-1} is due to the ν(O–H) stretching vibration of OH moieties involved in hydrogen bonds. Finally, the intense and sharp absorption at 1653 cm^{-1} is referred to the ν(C=O) stretching vibration.

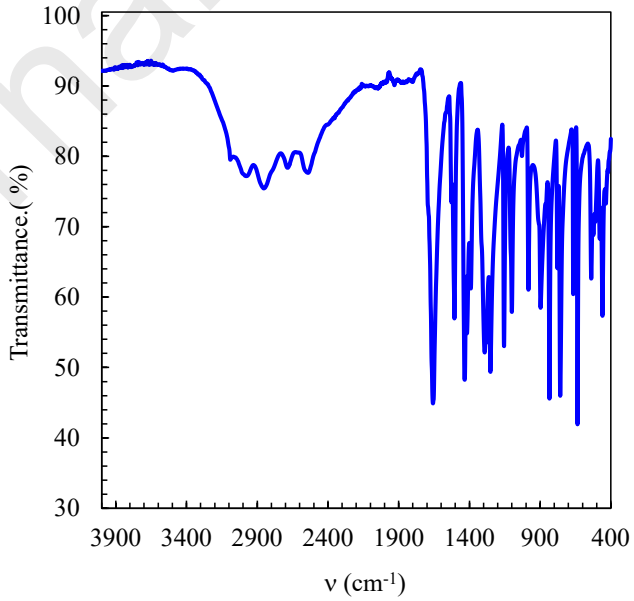

Figure 1. Infrared spectrum of **H_2TzPhTz**.

3.2. $Me_2TzPhTz{\cdot}2CF_3CO_2H$: structural characterization. Large colourless platelets of the trifluoroacetic adduct of dimethyl [2,2'-(1,4-phenylene)bithiazole]-5,5'-carboxylate (**$Me_2TzPhTz{\cdot}2CF_3CO_2H$**), grown by slow evaporation of a **$Me_2TzPhTz$** trifluoroacetic acid solution, were isolated and used for the structure determination. The analysis of the molecular structure and the pertinent geometrical parameters of **$Me_2TzPhTz{\cdot}2CF_3CO_2H$** has been carried out to gain information useful for the subsequent structural determination of **Zn_TzPhTz** from powder X-ray diffraction (*vide infra*). This compound crystallizes in the monoclinic space group $P2_1/n$. The asymmetric unit contains one ester molecule and two CF_3CO_2H molecules, in general positions. The **$Me_2TzPhTz$** molecule is almost planar: the dihedral angles subtended by the mean planes of the central phenyl ring and the heteroaromatic rings amount to 6.48(8) and 3.97(9)° (for the rings containing the S1 and S2 atoms, respectively; Figure 2a, showing the atom labels used throughout the discussion). The penta-atomic rings show a *trans* disposition of their heteroatoms, as observed in many other conjugated bis(heterocyclic) compounds such as 2,2′-biselenophene [35], 2,2′-biselenophene-5,5'-dicarboxylic acid [15], 2,2′-bithiazole [36], 2,2′-bithiophene [37] or 2,2′-bithiazole-5,5′-dicarboxylic acid [13]. The heteroatoms *trans* arrangement in π-conjugated compounds is presumably the lowest-energy conformation, granting the smallest steric hindrance. The two components of the molecular adduct are associated by means of hydrogen bonds (Figure 2a). Strong and directional OH···N interactions involving the thiazole nitrogen atoms are the strongest hydrogen bonds present in the crystal structure (see the caption to Figure 2 and Table S1 in the ESI). The difference between the two C-O bond lengths of the carboxylic group is a proof of evidence that the molecular components exist in their neutral forms and not as the ionic thiazolium trifluoroacetate salt: for both independent CF_3CO_2H molecules, the combinations of short [C17-O6 = 1.189(3) Å, C19-O8 = 1.192(3) Å] and long [C17-O5 = 1.291(4) Å, C19-O7 = 1.298(3) Å] bonds are typical of neutral carboxylic groups. The most interesting non-bonding interactions involve the carbonyl O2 and O4 atoms of **$Me_2TzPhTz$**, which form directional CH···O interactions (Figure 2b), accompanied by hypervalent S···O interactions [O4···S1#1 = 3.331(2) Å; S2···O1#1 = 3.275(2) Å; #1: *x*, *y*, *z*-1; Figure

2b] with the positively polarized sulphur atoms belonging to neighbouring **Me_2TzPhTz** molecules. These interactions assemble the diester molecules into strips down the crystallographic *c*-axis. As unveiled by a Hirshfeld surface analysis [38] for the individual **Me_2TzPhTz** molecules, the S···O/O···S contacts contribute as much as 6.7% to the entire surface and, therefore, they may be regarded as a perceptible supramolecular force. Weak intermolecular CH···O interactions (Figure 2a,b) are present among the **Me_2TzPhTz** and CF_3CO_2H molecules [C···O distances in the range 3.221(3)-3.378(2) Å]. Together with the hydrogen bonds quoted above, these interactions assemble the **Me_2TzPhTz** strips into 2-D layers parallel to the crystallographic *bc* plane (Figure 2b). Finally, CH···F interactions [C···F distances in the range 3.231(3)-3.530(4) Å; Figure 2c] and slipped π-π stacking interactions among inversion-related neighbouring **Me_2TzPhTz** molecules assemble the layers along the crystallographic *a*-axis [shortest C···C distance = 3.479(3) Å; distance between the centroids of phenylene rings = 3.848(3) Å; slippage angle = 25.75(8)°].

3.3. Zinc(II) and uranium(VI) coordination polymers containing H_2TzPhTz: synthesis and preliminary characterization. The Zn^{II} CP **Zn_TzPhTz** was obtained under solvothermal conditions reacting $Zn(CH_3COO)_2{\cdot}2H_2O$ and **H_2TzPhTz** in 1:1 molar ratio in DMF (**H_2TzPhTz** is sparingly soluble only in DMF). In the solid-state FT-IR spectrum of **Zn_TzPhTz** (Figure 3), the disappearance of the very broad ν(O–H) signal between 2900 and 2200 cm^{-1} observed in the spectrum of the ligand (Figure 1) and the shift of the ν(C=O) band toward lower wavenumbers with respect to the ligand (from 1653 to 1560 cm^{-1}) are in accordance with the deprotonation of the spacer and the coordination of its carboxylate groups to the metal ion, as confirmed by the structure determination. Moreover, the lower number of bands observed in the fingerprint region of **Zn_TzPhTz** with respect to the free ligand indicates a reduction of the ligand vibrational degrees of freedom when incorporated within the coordination polymer. The thermogravimetric analysis, carried out under nitrogen atmosphere, showed that **Zn_TzPhTz** is stable up to 540 K (Figure 4).

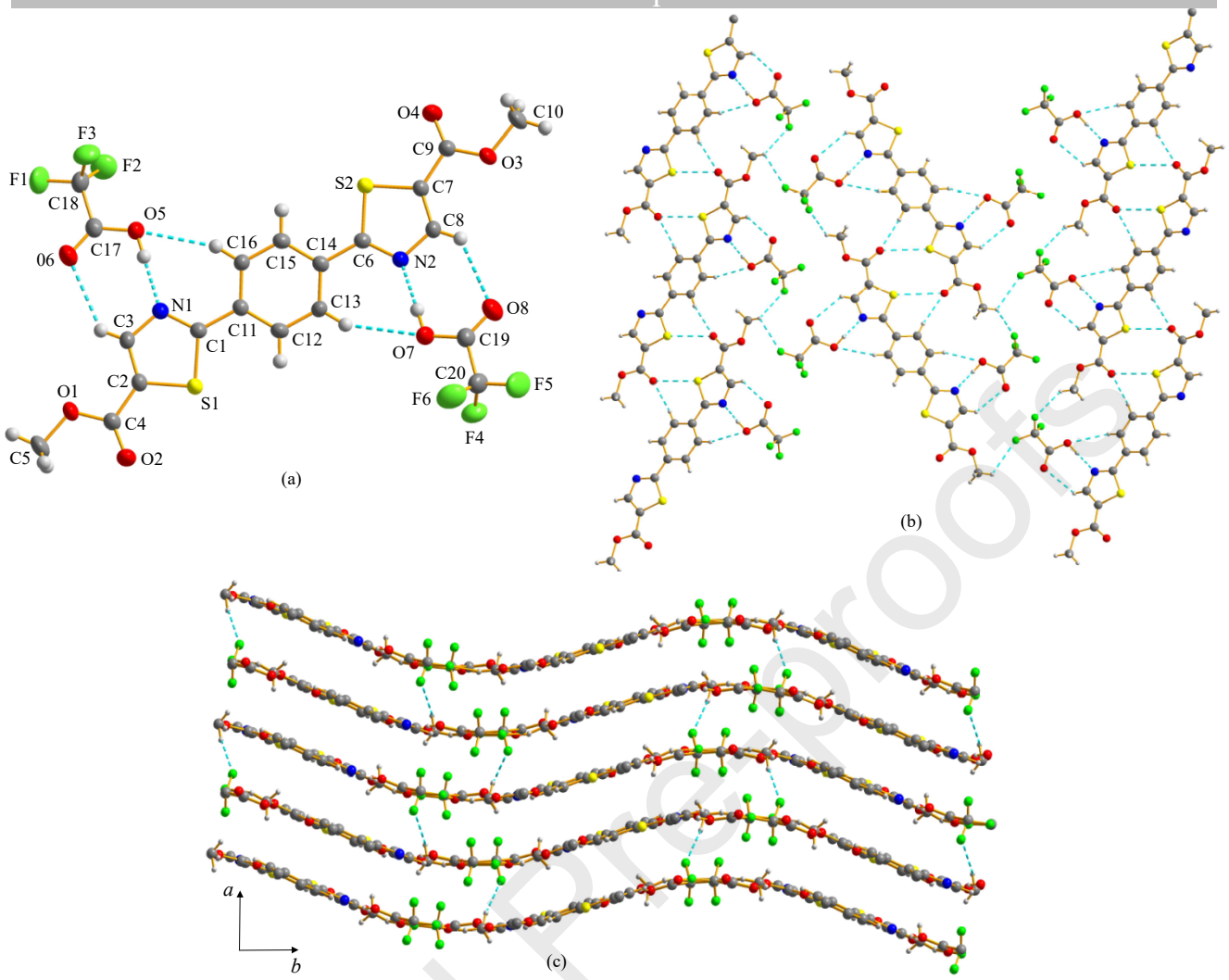

Figure 2. Representation of the crystal structure of **$Me_2TzPhTz{\cdot}2CF_3CO_2H$**: a) the molecular structure, with thermal ellipsoids drawn at the 50% probability level. The dotted blue lines indicate the OH···N [O5···N1, 2.669(2) Å; O7···N2, 2.649(2) Å; O-H···N, 167.7, 172.5°] and CH···O non-bonding interactions. b) Portion of a 2-D layer, showing the OH···N, CH···O, CH···F and S···O non-bonding interactions. c) Packing of the 2-D layers along the crystallographic *a*-axis, driven by CH···F interactions (dotted blue lines) and slipped π-π stacking interactions (not shown). Atom colour code: carbon, grey; hydrogen, light grey; fluorine, light green; nitrogen, blue; oxygen, red; sulphur, yellow.

The progressive weight loss of ca 9% in the temperature range 300-500 K can be ascribed to the loss of two coordinated water molecules *per* formula unit (calculated mass loss = 8.3%). Thermal decomposition starts after this event in the temperature range 540-680 K. At the end of the decomposition (900 K) a black residue, corresponding to *ca*. 24% of the initial weight, is recovered. A qualitative analysis

on the PXRD data of the residue revealed its chemical identity as zinc(II) sulfide, ZnS (calculated residual mass = 22.5%) (Figure S3).

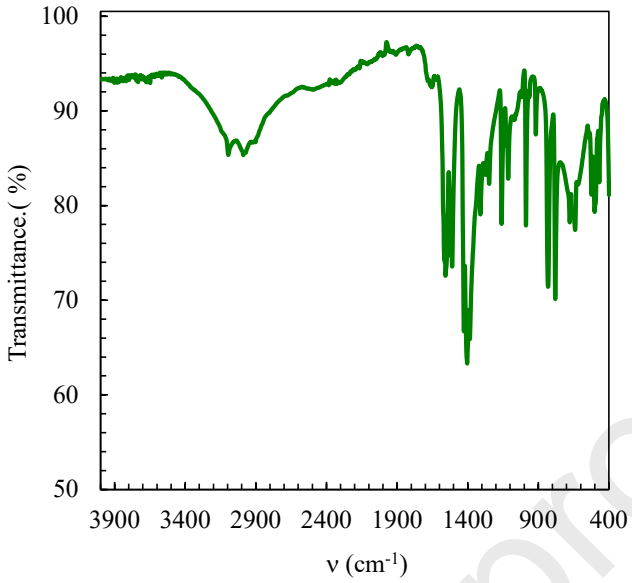

Figure 3. Infrared spectrum of **Zn_TzPhTz**.

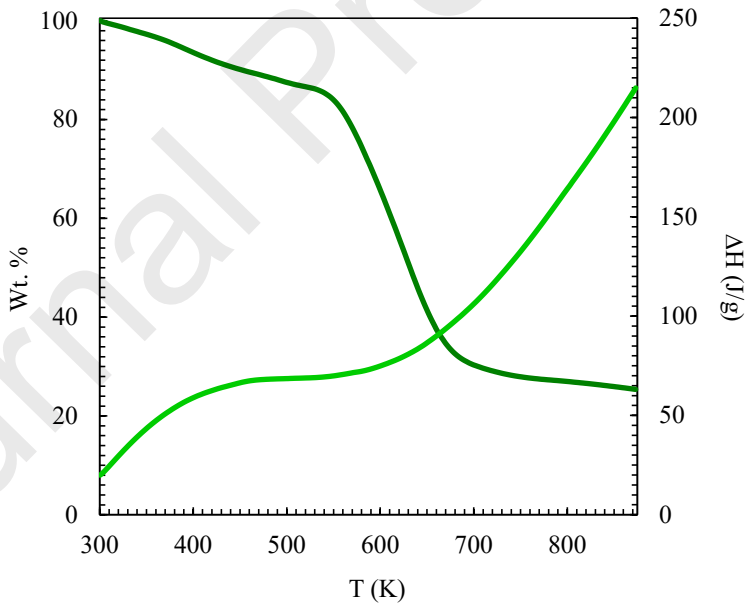

Figure 4. Thermogravimetric analysis (green curve) and differential thermal analysis (light green curve) for **Zn_TzPhTz**.

Crystals of **U_TzPhTz** were obtained under solvothermal conditions in DMF. The reaction was performed at 413 K, 373 K and 353 K, yielding in all cases mixtures of **U_TzPhTz** and a dark unidentified

material. The best results were obtained when the reaction mixture (20% excess amount of the ligand) was heated at 413 K for 48 h. Despite the numerous attempts, we could never prepare the pure compound.

3.3. Zinc(II) and uranium(VI) coordination polymers: crystal and molecular structure. Compound **Zn_TzPhTz** crystallizes in the monoclinic space group *Pc*. The asymmetric unit contains one Zn^{II} ion, one **TzPhTz**$^{2-}$ ligand and two water molecules, in general positions, forming a mono-dimensional coordination polymer with **2C1** topology (taking the Zn^{II} ion as node and **TzPhTz**$^{2-}$ as spacer) [39]. The metal ion is hexa-coordinated and shows a *cis*-$\{Zn(O_{TzPhTz})_4(O_{H2O})_2\}$ octahedral stereochemistry (Figure 5a): the distorted octahedron [O-Zn-O = 54.46(14)-154.49(30)°] is defined by the oxygen atoms of two chelating carboxylate groups, with one long Zn-O distance, and by the oxygen atoms of two *cis*–positioned water molecules (see Figure 3a and its caption for the bond distances and angles). These nodes are connected by μ-η^2(O1,O2):η^2(O3,O4)-**TzPhTz**$^{2-}$ ligands, lying approximately about the (2 1 0) crystallographic plane, along zig-zag chains (Figure 5b) [Zn···Zn = 18.420(7) Å] running parallel to the [-1 0 -2] crystallographic direction (Figure 5c) (in accordance with the preferred orientation found along the [1 0 -2] pole). The two thiazole heteroatoms in the ligand show a reciprocal *trans* disposition with respect to the central phenyl ring, as observed in the bare **Me$_2$TzPhTz** (*vide supra*). In **Zn_TzPhTz** the heterocyclic rings are not strictly coplanar, showing a deviation of 1.3°. Each water molecule is involved in two hydrogen bonds toward two neighbouring chains, one with the heterocyclic nitrogen atom and one with the oxygen atom of one carboxylate group (see Figure 5d and its caption). Moreover, π-π interactions among the hexa- and penta-atomic rings of neighbouring chains are at work (shortest C-C distance = 3.63 Å, centroid to centroid distances = 3.60, 3.65 Å). Each chain is thus connected to seven nearby ones, yielding a three-dimensional supramolecular architecture. No S···O interactions are present, at variance with **Me$_2$TzPhTz·2CF$_3$CO$_2$H**.

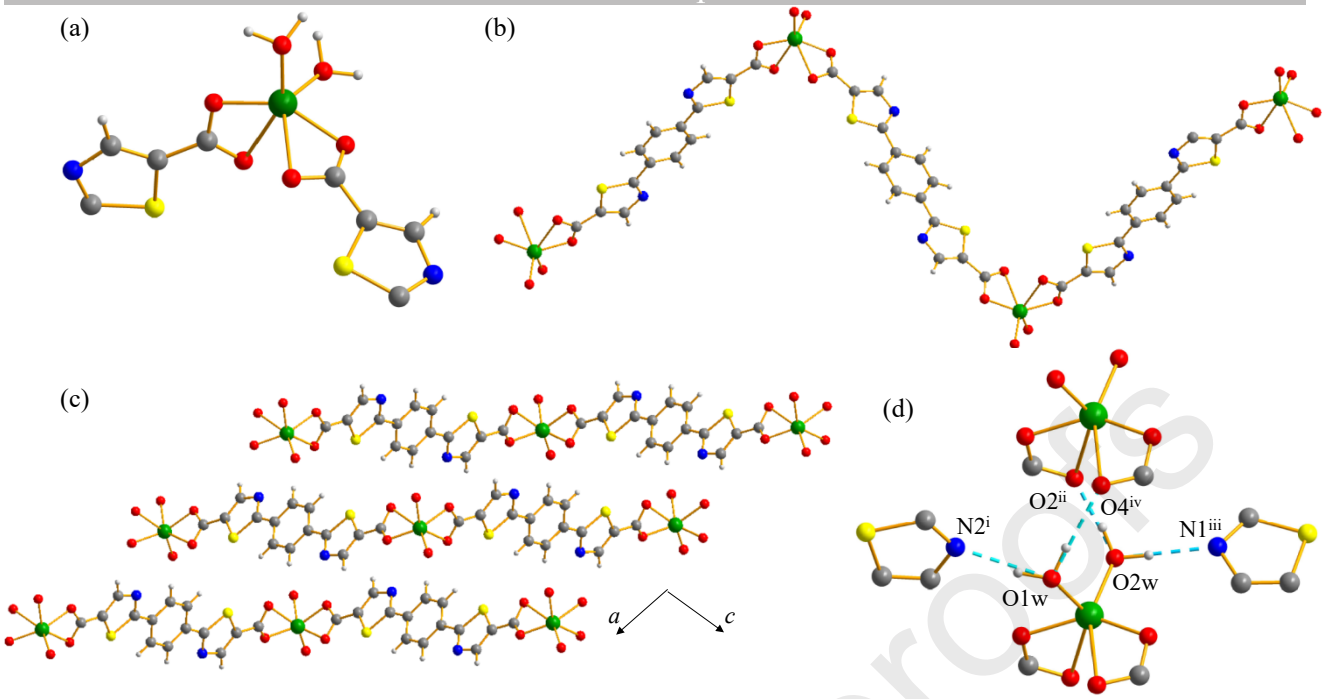

Figure 5: Representation of the crystal structure of **Zn_TzPhTz**: a) the stereochemistry of the Zn^{II} ion; b) portion of the 1-D polymeric motif; c) portion of the crystal packing viewed along the crystallographic *b*-axis. d) The hydrogen bonds involving the water molecules (cyan dotted lines). Atom colour code: carbon, grey; hydrogen, light grey; nitrogen, blue; oxygen, red; sulphur, yellow; zinc, green. Main bond distances and angles at the metal ion: Zn-O1w, 2.058(5) Å; Zn-O2w, 1.961(6) Å; Zn-O1, 1.914(6) Å; Zn-O2, 2.616(5) Å; Zn-O3, 2.009(6) Å; Zn-O4, 2.441(5) Å; O-Zn-O, 54.46(14)-154.49(30)°. Hydrogen bonds: O1w···$N2^{i}$, 2.8611(1) Å; O1w-H···$N2^{i}$, 168°; O1w···$O4^{ii}$, 2.4917(1) Å; O1w-H···$O4^{ii}$, 150°; O2w···$N1^{iii}$, 2.8231(1) Å; O2w-H···$N1^{iii}$, 166°; O2w-H···$O2^{iv}$, 3.0233(1); O2w-H···$O2^{iv}$, 171°. Symmetry operations: (i) -1+x, -y, -1/2+z; (ii) -1+x, y, z; (iii) x, -1+y, z; (iv) x, 1-y, -1/2+z. For the labels, the reader is addressed to Scheme S1 of the ESI.

U_TzPhTz crystallizes in the triclinic space group *P*-1. The asymmetric unit contains an U^{VI} ion, two O^{2-} anions, one **$TzPhTz^{2-}$** spacer and two DMF molecules, in general positions. The uranium(VI) ions exhibit the typical coordination number seven in a distorted pentagonal bipyramidal geometry [40] with two O^{2-} ligands occupying the axial positions [Figure 6a; U-O = 1.752(3), 1.757(3) Å; see the caption to Figure 6 for the bond distances and angles]. The equatorial positions of the coordination polyhedron are occupied by five oxygen atoms coming from two carboxylate groups of two **$TzPhTz^{2-}$** ligands, one chelating carboxylate group of another **$TzPhTz^{2-}$** ligand and one DMF molecule [U-O = 2.333(3)-2.481(3) Å]. Pairs of carboxylate bridges assemble the metal ions into centrosymmetric dimers (Figure

6a), with a U1···U1^{i} separation of 5.4986(5) Å [symmetry operation: (i) 2-*x*, -*y*, -*z*]. The formation of dimers is a recurring motif for a number of UO_2^{2+}/carboxylate systems [41]. Similarly to some of the molecular prototypes with the $[(UO_2)_2(\mu\text{-}RCO_2)_2(RCO_2)_2(L)_2]$ (L = H_2O, DMF, Ph_3PO) dimers, the dimers in **U_TzPhTz** accommodate two additional oxygen-donor molecules (namely DMF) [42]. When combined with dicarboxylate ligands, these dimers may be viewed as supramolecular synthons for the generation of coordination polymers. However, examples of the assembling of such motifs into coordination polymers are relatively rare [43]. In **U_TzPhTz**, pairs of μ^2(O5,O6):μ-η^2(O3,O4)-**TzPhTz**$^{2-}$ ligands connect the dimers (distance between the dimers centroids = 18.88 Å) to yield 1-D coordination polymers running approximately along the [0 1 1] crystallographic direction (Figure 6b). Instead of an open four-connected array, which would be anticipated for the combination of dimeric nodes and dicarboxylate spacers in 1:2 proportions, each couple of neighboring dimers is bridged by two **TzPhTz**$^{2-}$ linkers (Figure 6b), thus decreasing the dimensionality of the crystal structure to 1-D, with a **(4,4)(0,2)** network topology (taking the U^{VI} ion as node and **TzPhTz**$^{2-}$ as spacer) [39]. The double **TzPhTz**$^{2-}$ linkage is primarily conditioned by its conformational flexibility, where the thiazole ring heteroatoms are in a *cis* conformation, contrarily to what observed in **Me$_2$TzPhTz**·2CF_3CO_2H and **Zn_TzPhTz**. This conformational flexibility implies a collapse of the potentially obtainable 2-D layer into a 1-D polymeric architecture. The generation of topologically identical 1-D double-bridged arrays of $[(UO_2)_2(\mu\text{-}RCO_2)_2(RCO_2)_2(L)_2]$ units has been observed also for geometrically rigid ligands, such as 1,3-adamantanedicarboxylate [44] and the trimesic acid dianion in two very similar structures with L = H_2O [45]. At variance with **Me$_2$TzPhTz·2CF$_3$CO$_2$H**, in **U_TzPhTz** there are no short S···O interactions. This may be attributed to the steric inaccessibility of the sulphur atoms due to the formation of double dicarboxylate bridges.

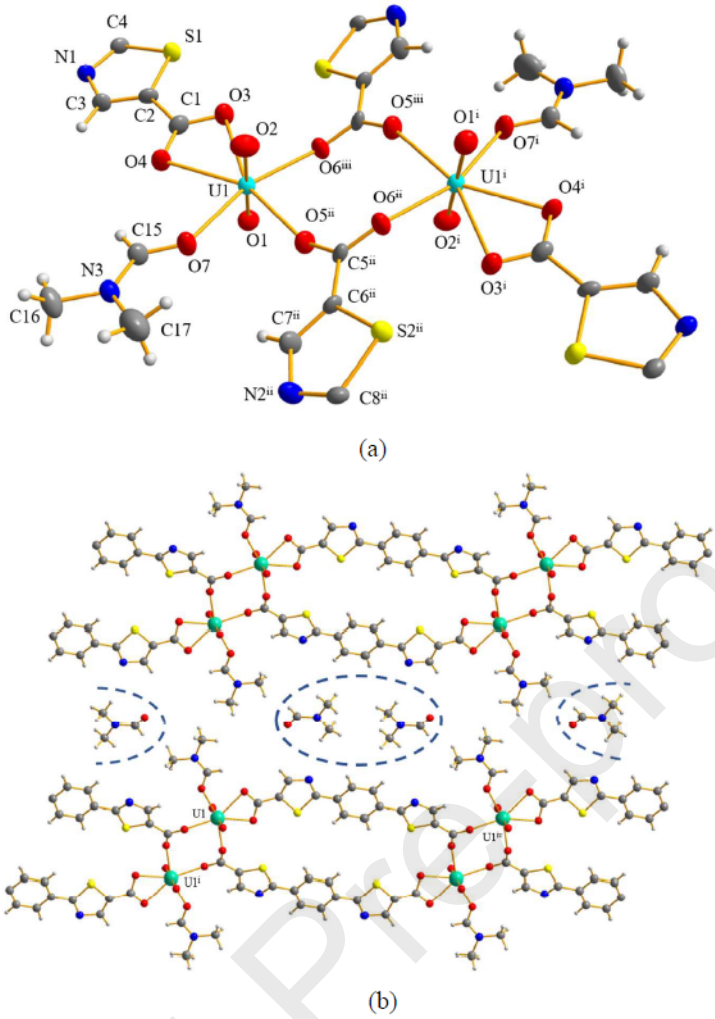

Figure 6. Representation of the crystal structure of **U_TzPhTz**: a) the dimer, supported by one pair of μ-carboxylate groups and mediated by pairs of chelating carboxylates and DMF molecules (50% probability ellipsoids). b) Packing of the 1-D chains: in between, highlighted with blue dotted lines, the chlatrated DMF molecules. Atoms colour code: carbon, grey; hydrogen, light grey; oxygen, red; nitrogen, blue; sulfur, yellow; uranium, cyan. Main bond distances and angles at the metal ion: U1-O1, 1.752(3) Å; U1-O2, 1.757(3) Å; U1-O3, 2.435(3) Å; U1-O4, 2.481(3) Å; U1-O5^{ii}, 2.333(3) Å; U1-O6^{iii}, 2.339(3) Å; U1-O7, 2.360(3) Å; O1-U1-O2, 179.68(16)°; O3-U1-O4, 53.04(9)°; O4-U1-O7, 72.85(9)°; O7-U1-O5^{ii}, 78.96(10)°; O3-U1-O6^{iii}, 73.37(10)°; O5^{ii}-U1-O6^{iii}, 82.04(10)°. Symmetry operations: (i) 2-*x*, -*y*, -*z*; (ii) *x*, -1+*y*, -1+*z*; (iii) 2-*x*, 1-*y*, 1-*z*; (iv) *x*, 1+*y*, 1+*z*.

3.4. Comparative structural analysis. Inspired by the review published in 2019 [46] proposing a literature survey of zinc(II) and cadmium(II) coordination polymers with thiazole linkers appeared in the period 2015–2019, we performed a comprehensive search in the Cambridge Structural Database (CSD)

[20] for Zn^{II} and U^{VI} coordination polymers containing that kind of linkers. No uranium(VI) thiazole-containing coordination polymers could be found, but only one coordination complex [47]. On the contrary, we found eleven coordination polymers with zinc(II). For ten of them [48], the crystallographic information was retrieved from the CSD, while for one of them reference was made to the original paper [49]. Of these compounds, five are one-dimensional coordination polymers, like the title one, while two show two-dimensional, and three show three-dimensional polymeric architectures. Within the 1-D coordination polymers, $[Zn(TTz)(H_2O)_2]$ (H_2TTz = thiazolo[5,4-d]thiazole-2,5-dicarboxylic acid) [48e] shows the same **2C1** topology found in **Zn_TzPhTz**. The metal centre is tetra-, penta- or hexa-coordinated with tetrahedral (four occurrences; τ_4 = 0.86-0.90; coordination sphere of the kind ZnO_3N or ZnO_4; Zn-O distances 1.90–2.01 Å), square pyramidal (eight occurrences; τ_5 = 0.01-0.15; coordination sphere of the kind ZnO_5, ZnO_4N or ZnO_3N_2; Zn-O distances 1.99-2.14 Å), trigonal bipyramidal (one occurrence; τ_5 = 0.60; coordination sphere of the kind ZnN_2O_3; Zn-O distances 1.93-2.00 Å), or octahedral geometry (three occurrences; coordination sphere of the kind ZnO_6 or *trans*-ZnF_2NO_3; Zn-O distances 1.91-2.62 Å), respectively. On the whole, the coordination sphere of the metal centre is defined by the oxygen, nitrogen or fluorine donor atoms of the different ligands present. As anticipated before, in **Zn_TzPhTz** the Zn^{II} ion has coordination number six and shows a *cis*-$\{Zn(O_{TzPhTz})_4(O_{H2O})_2\}$ octahedral stereochemistry, with Zn-O distances in the range 1.961(6)-2.616(5) Å, matching those of the literature compounds quoted above possessing the same stereochemistry. As for the thiazole ligands of our search, it emerged that they can be monodentate (five cases, exclusively in 1-D coordination polymers), exo-bidentate (five cases) and exo-tridentate (three cases), with no chelating examples. At variance, in **Zn_TzPhTz** both carboxylate groups are chelating.

For the sake of completeness, we compare here the main features of the complex $[UO_2(H_2O)_2(PyTz)_2]$ [HPyTz = 2-(pyridin-4-yl)-1,3-thiazole-4-carboxylic acid] [47] with those of **U_TzPhTz**. In the former, the U^{VI} ion shows coordination number eight in *trans*-hexagonal bipyramidal coordination geometry, with the O^{2-} anions in the axial positions, with U-O distances in the range 1.78-2.50 Å. The nature of the ligand,

possessing only one carboxylate group, and the fact that it chelates the metal centre, does not allow the formation of oligomeric or polymeric motifs, thus being completely different from **U_TzPhTz**, in terms of stereochemistry at the metal ion and dimensionality of the structural motif.

3.5. Luminescence properties of H_2TzPhTz and Zn_TzPhTz. With the luminescence sensing target in mind for MOFs (i.e. 3-D porous coordination polymers) built with **H_2TzPhTz**, we examined the absorption and emission properties of the free ligand **H_2TzPhTz** and of **Zn_TzPhTz** in the solid state. The absorption spectrum of **H_2TzPhTz** (Figure 7) is featured by a broad band centred at λ = 351 nm, red-shifted with respect to that found for the shorter analogue H_2TzTz ($\lambda \approx$ 325 nm).[15] The red shift is likely caused by the more extended π-conjugation due to the introduction of a phenyl ring between the two thiazole rings. Upon excitation at 350 nm, the emission spectrum of **H_2TzPhTz** shows a maximum at λ = 474 nm (Figure 7), generating a blue-green colour upon excitation under a UV lamp (see inset in Figure 7 for the CIE chromatic coordinates). In the case of **Zn_TzPhTz**, the absorption maximum is found at λ = 326 nm (Figure 8), falling in the same spectral region found for **H_2TzPhTz**. The electronic transition is of $\pi \rightarrow \pi^*$ or $n \rightarrow \pi^*$ nature and it is ligand-centred, since the metal ion, with its d^{10} closed-shell configuration, is not involved in metal-to-ligand or ligand-to-metal charge transfers. In line with this statement and with other literature examples of Zn^{II} thiazole-based CPs,[48a,48f] upon excitation at 325 nm the emission spectrum is featured by a peak at λ = 477 nm (Figure 8), and is practically identical to that of the free linker, falling again in the blue-green visible region (see inset in Figure 8 for the CIE chromatic coordinates).

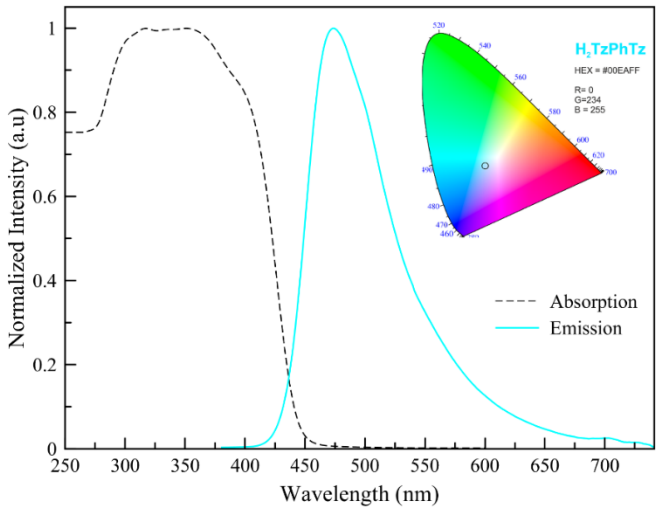

Figure 7. Comparison between the normalized absorption (dotted black line) and the emission (blue-green line) spectra (λ_{ex} = 350 nm) of **H_2TzPhTz** as powder at r.t. Inset: CIE diagram derived from the emission spectrum, with hexadecimal (HEX) and RGB coordinates of the corresponding emission color.

Figure 9 shows the real samples emission at comparison under an ordinary UV lamp. The absolute emission intensity of the zinc(II) polymer is higher than that of the free ligand. This has already been observed in other luminescent MOFs and CPs of the literature: the insertion of the emissive linker within a rigid crystalline framework limits the occurrence of self-quenching effects.[46]

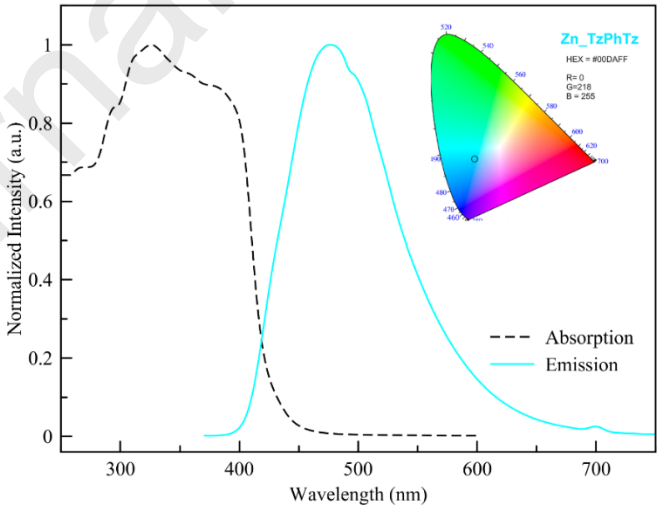

Figure 8. Comparison between the normalized absorption and the emission spectra (λ_{ex} = 325 nm) of **Zn_TzPhTz** as powder at r.t. Inset: CIE diagram derived from the emission spectrum, with hexadecimal (HEX) and RGB coordinates of the corresponding emission color.

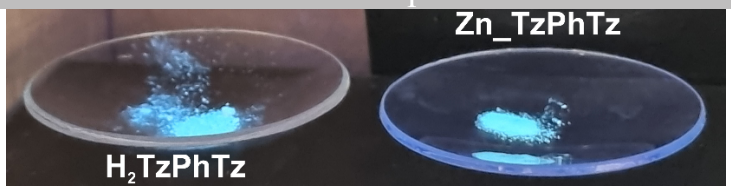

Figure 9. Photograph of **H_2TzPhTz** and **Zn_TzPhTz** powders emission under a UV lamp at comparison.

4. Conclusions

Performing a classical Hantzsch synthesis, we have prepared the new linker [2,2'-(1,4-phenylene)bithiazole]-5,5'-carboxylic acid (**H_2TzPhTz**) in ~70% yield. Its coordination versatility toward representative *d* (Zn^{II}) and *f* (U^{VI}) transition metal ions led to the isolation of the coordination polymers $[Zn(TzPhTz)(H_2O)_2]$ and $[UO_2(TzPhTz)(DMF)]\cdot DMF$. Both are characterized by 1-D chains with *cis*-$\{Zn(O_{COO})_4(O_{H2O})_2\}$ and $\{UO_2(O_{COO})_4(O_{DMF})\}_2$ nodes, respectively. **H_2TzPhTz** emits in the blue-green visible region, as well as the Zn^{II} coordination polymer, proving that in the latter the electronic transitions involved are ligand-centred. The obtained results must be considered propaedeutic to the preparation of 3-D MOFs containing this linker properly "diluted" in a non-emissive matrix to be exploited in luminescence sensing applicative contexts. Ongoing activity in this direction is being carried out in our laboratories at present.

Supporting Information. Hydrogen sulphide production (Paragraph S1). Thermogravimetric analysis and differential thermal analysis of **Me_2TzPhTz** (Figure S1). Graphical representation of the final structure refinement stage for **Zn_TzPhTz** (Figure S2). Powder X-ray diffraction data of the residue recovered after TGA analysis on **Zn_TzPhTz**. (Figure S3). Hydrogen bond geometry of **Me_2TzPhTz** and **U_TzPhTz** (Tables S1 and S2). Atom labels of **Zn_TzPhTz** (Scheme S1).

Conflicts of interest

The authors declare no conflicts of interest.

ORCID

Simona Galli: 0000-0003-0335-5707

Giuliano Giambastiani: 0000-0002-0315-3286

Giorgio Mercuri: 0000-0002-2467-6342

Marco Moroni: 0000-0001-6167-3792

Andrea Rossin: 0000-0002-1283-2803

Corrado Di Nicola: 0000-0002-0958-6103

Patrizio Campitelli: 0000-0001-6950-0626

Acknowledgments. SG, SB and MM acknowledge Università dell'Insubria for partial funding and Miss Lisa Proserpio for experimental help. This work was supported by the National Research Foundation of Ukraine (Project no. 2020.02/0071). MP, GG and AR would like to thank the Italian MIUR through the PRIN 2017 project MULTI-e (20179337R7) "Multielectron transfer for the conversion of small molecules: an enabling technology for the chemical use of renewable energy" and the TRAINER project "Catalysts for Transition to Renewable Energy Future" (Ref. ANR-17-MPGA-0017) for financial support. AR is deeply grateful to Dr. Alessio Dessì (ICCOM-CNR) for his invaluable help in collecting the UV-Vis spectra.

References

Coordination polymers of *d*- and *f*-elements with (1,4-phenylene)dithiazole dicarboxylic acid

Kostiantyn V. Domasevich,[a] Patrizio Campitelli,[b] Marco Moroni,[c] Simona Bassoli,[c]

Giorgio Mercuri,[d,e] Matteo Pugliesi,[d] Giuliano Giambastiani,[d]

Corrado Di Nicola,[e,] Andrea Rossin[d,]* and Simona Galli[c,]**

[a] Taras Shevchenko National University of Kyiv
Volodymyrska Str. 64/13, 01601 Kyiv, Ukraine.

[b] Scuola del Farmaco e dei Prodotti della Salute, Università di Camerino,
Via S. Agostino 1, 62032 Camerino, Italy.

[c] Dipartimento di Scienza e Alta Tecnologia, Università dell'Insubria,
Via Valleggio 11, 22100 Como, Italy.

[d] Istituto di Chimica dei Composti Organometallici (ICCOM-CNR),
Via Madonna del Piano 10, 50019 Sesto Fiorentino, Italy.

[e] Scuola di Scienze e Tecnologie, Università di Camerino,
Via S. Agostino 1, 62032 Camerino, Italy.

Authors to whom correspondence should be addressed:

Prof. Simona Galli (simona.galli@uninsubria.it);

Dr. Corrado Di Nicola (corrado.dinicola@unicam.it);

Dr. Andrea Rossin (a.rossin@iccom.cnr.it).

Highlights

- 2,2'-(1,4-phenylene)dithiazole-5-carboxylic acid (H_2TzPhTz) has been prepared for the first time *via* the classical Hantzsch synthesis
- [Zn(TzPhTz)(H_2O)$_2$] shows hydrogen-bonded 1-D zig-zag chains with *cis*-{Zn(O_{COO})$_4$(O_{H2O})$_2$} nodes and μ-η^2:η^2-TzPhTz spacers
- [UO_2(TzPhTz)] features {UO_2(TzPhTz)(DMF)}$_2$ dimeric units along 1-D strands

[1] See e.g. a) O.M. Yaghi, M.J. Kalmutzki, C.S. Diercks, Introduction to Reticular Chemistry: Metal-Organic Frameworks and Covalent Organic Frameworks, VCH Verlagsgesellschaft Mbh, 2019. b) S. Kaskel, The Chemistry of Metal–Organic Frameworks: Synthesis, Characterization, and Applications, Wiley-VCH, 2016. c) S.R. Batten, B. Chen, J.J. Vittal Eds., ChemSusChem 81 (2016) 669-670. d) S.R. Batten, S.M. Neville, D.R. Turner, Coordination Polymers: Design, Analysis and Application, RSC Publishing, 2009. e) M.C. Hong, L. Chen Eds., Design and construction of coordination polymers, John Wiley & Sons, Hobokey, New Jersey, 2009.

[2] P.Z. Moghadam, A. Li, X.-W. Liu, R.B. Perez, S.-D. Wang, S.B. Wiggin, P.A. Wood, D. Fairen-Jimenez, Chem. Sci. 11 (2020) 8373-8387.

[3] See e.g.: a) H. García, S. Navalón Eds., Metal-Organic Frameworks: Applications in Separations and Catalysis, Wiley-VCH, 2018. b) B. Chen, G. Qian Eds., Metal-Organic Frameworks for Photonics Applications, Springer-Verlag, Berlin, Heidelberg, 2014. c) D. Farrusseng Ed., Metal-Organic Frameworks: Applications from Catalysis to Gas Storage, Wiley-VCH, 2011.

[4] A.R. Katritzky, C.A. Ramsden, E.F.V. Scriven, R.J.K. Taylor Eds., Comprehensive heterocyclic chemistry III, Elsevier, Amsterdam, 2008.

[5] a) Y. Bai, Y. Dou, L.-H. Xie, W. Rutledge, J.-R. Li, H.-C. Zhou, Chem. Soc. Rev. 45 (2016) 2327-2367. b) S.-Q. Bai, D.J. Young, T.S. Andy Hor, Chem. Asian J. 6 (2011) 292-304.

[6] a) S.S. Chen, CrystEngComm 18 (2016) 6543-6565. b) B. Chen, Z. Yang, Y. Zhu, Y. Xia, J. Mater. Chem. A 2 (2014) 16811-16831.

[7] a) C. Pettinari, A. Tăbăcaru, S. Galli, Coord. Chem. Rev. 307 (2016) 1-31. b) M. Viciano-Chumillas, S. Tanase, L.J. de Jongh, J. Reedij, Eur. J. Inorg. Chem. (2010) 3403-3418.

[8] G. Aromí, L.A. Barrios, O. Roubeau, P. Gamez, Coord. Chem. Rev. 255 (2011) 485–546.

[9] a) A. Tăbăcaru, C. Pettinari, S. Galli, Coord. Chem. Rev. 372 (2018) 1–30. b) H. Zhao, Z.-R. Qu, H.-Y. Ye, R.-G. Xiong, Chem. Soc. Rev. 37 (2008) 84-100.

[10] X. Li, W. Ma, H. Li, Q. Zhang, H. Liu, Coord. Chem. Rev. 408 (2020) 213191.

[11] H.-Y.Wang, L. Cui, J.-Z. Xie, C.F. Leong, D.M. D'Alessandro, J.-L. Zuo, Coord. Chem. Rev. 345 (2017) 342-361.

[12] G. Mercuri, G. Giambastiani, C. Di Nicola, C. Pettinari, S. Galli, R. Vismara, R. Vivani, F. Costantino, M. Taddei, C. Atzori, F. Bonino, S. Bordiga, B. Civalleri, A. Rossin, Coord. Chem. Rev. 437 (2021) 213861.

[13] P. Müller, B. Bucior, G. Tuci, L. Luconi, J. Getzschmann, S. Kaskel, R.Q. Snurr, G. Giambastiani, A. Rossin, Mol. Syst. Des. Eng. 4 (2019) 1000-1013.

[14] Baran, Richter, Essentials of Heterocyclic Chemistry - I.

[15] G. Mercuri, M. Moroni, A. Fermi, G. Bergamini, S. Galli, G. Giambastiani, A. Rossin, Inorg Chem. 59 (2020) 15832–15841.

[16] a) J.E. Mulvaney, C.S. Marvel, J. Org. Chem. 26 (1961) 95-97. b) G. Maier, R. Hecht, Macromol. 28 (1995) 7558-7565.

[17] A.A. Coelho, J. Appl. Crystallogr. 36 (2003) 86-95.

[18] TOPAS-R v.3, Karlsruhe, Germany, 2005.

[19] A. Le Bail, H. Duroy, J.L. Fourquet, Materials Research Bulletin 23 (1988) 447-452.

[20] Cambridge Crystallographic Data Center, 2021.

[21] Hexa-atomic ring: C-C = 1.39 Å, C-H = 0.95 Å; internal and external angles = 120°; exocyclic C-C distances: 1.49 Å; thiazolic rings: S_1-C_8 = 1.72 Å, S_1-C_7 = 1.69 Å, C_7-N_1 = 1.33 Å, N_1-C_9 = 1.35 Å, C_9-C_8 = 1.35 Å; C_7-S_1-C_8 = 89°, S_1-C_7-N_1 = 115°, C_7-N_1-C_9 = 110°, = N_1-C_9-C_8 = 116°, C_9-C_8-S_1 = 110°; carboxylate groups: C-O = 1.25 Å, O-C-O = 120°. For the molecular structure and the labels of the ligands the reader is addressed to Scheme S1 of the ESI.

[22] A.A. Coelho, J. Appl. Crystallogr. 33 (2000) 899-908.

[23] R.W. Cheary, A.A. Coelho, J. Appl. Crystallogr. 25 (1992) 109-121.

[24] a) A.Z. March, Z. Kristallogr. 81 (1932) 285-297; b) W.A. Dollase J. Appl. Crystallogr. 19 (1986) 267-272.

[25] IUCr Monograph N. 5. R.A. Young, Oxford University Press, New York, 1981.

[26] K. Brandenburg, Diamond 2.1e, Crystal Impact GbR, Bonn, 1999.

[27] X-RED, Version 1.22, Stoe & Cie GmbH, Darmstadt, Germany, 2001.

[28] X-SHAPE, Revision 1.06, Stoe & Cie GmbH, Darmstadt, Germany, 1999.

[29] G.M. Sheldrick, Acta Crystallogr. A64 (2008) 112–122.

[30] G.M. Sheldrick, Acta Crystallogr. C71 (2015) 3-8.

[31] a) A. Hantzsch, J.H. Weber, Dtsch. Chem. Ges. 20 (1887) 3118-3132. b) R.H. Wiley, D.C. England, L.C. Behr, Org. Reac. 6 (1951) 367-409.

[32] a) J.E. Mulvaney, C.S. Marvel, J. Org. Chem. 26 (1961) 95-97. b) G. Maier, R. Hecht, Macromol. 28 (1995) 7558-7565.

[33] K.A. Abbas, J.T. Edward, Can. J. Chem. 63 (1985) 3075-3078.

[34] H.E. Faith, US Patent (1944) 2405820.

[35] S. Inoue, T. Jigami, H. Nozoe, Y. Aso, F. Ogura, Heterocycles 52 (2000) 159-170.

[36] D.C. Craig, H.A. Goodwin, D. Onggo, A.D. Rae, Aust. J. Chem. 41 (1988) 1625-1644.

[37] M. Pelletier, F. Brisse, Acta Crystallogr. Sect. C C50 (1994) 1942-1945.

[38] M.J. Turner, J.J. McKinnon, S.K.Wolff, D.J. Grimwood, P.R. Spackman, D. Jayatilaka, M.A. Spackman (2017). CrystalExplorer17. University of Western Australia. http://crystalexplorer.scb.uwa.edu.au/, last accessed January 2022.

[39] https://topcryst.com/, last accessed January 2022.

[40] J.J. Katz, G.T. Seaborg, L.R. Morss, The Chemistry of the Actinide Elements, 2nd ed., Vol. 1, pp. 169–442. London: Chapman and Hall, 1986.

[41] T. Loiseau, I. Mihalcea, N. Henry, C. Volkringer, Coord. Chem. Rev. 266–267 (2014) 69–109.

[42] A. Navaza, M.G. Iroulart, M. Nierlich, M. Lance, J. Vigner, Acta Crystallogr. Sect. C – Struct. Commun. 49 (1993) 1767–1770.

[43] P. Thuery, Eur. J. Inorg. Chem (2006) 3646–3651.

[44] J.A. Rusanova, E.B. Rusanov, K.V. Domasevitch, Acta Crystallogr. Sect. C – Struct. Chem. 66 (2010) m207–m210.

[45] L.A. Borkowski, C.L. Cahill, Acta Crystallogr. Sect. E – Crystallogr. Commun. 60 (2004) m198–m200.

[46] G. Mercuri, G. Giambastiani, A. Rossin, Inorganics 12 (2019) 144.

[47] R.C. Severance, S.A. Vaughn, M.D. Smith, H.-C. zur Loye, Solid State Sci. 13 (2011) 1344-1353. CSD Code OROLAJ.

[48] (a) S. Staderini, G. Tuci, M. D'Angelantonio, F. Manoli, I. Manet, G. Giambastiani, M. Peruzzini, A. Rossin, ChemistrySelect 6 (2016) 1123–1131. (b) T. Tao, X.-X. Wang, Y.-N. Wange, Z.-Y. Lu, W. Huang, Inorg. Chem. Commun. 31 (2013) 62-65. (c) X.-D. Chen, H.-F. Wu, X.-H. Zhao, X.-J. Zhao, M. Du, Cryst. Growth Des. 7 (2007) 124-131. (d) J.M. Ellsworth, C.-Y. Su, Z. Khaliq, R.E. Hipp, A.M. Goforth, M.D. Smith, H.-C. zur Loye, J. Mol. Struct. 796 (2006) 86-94. (e) A. Aprea, V. Colombo, S. Galli, N. Masciocchi, A. Maspero, G. Palmisano, Solid State Sci. 12 (2010) 795-802. (f) S. Staderini, G. Tuci, L. Luconi, P. Müller, S. Kaskel, A. Eychmüller, F. Eichler, G. Giambastiani, A. Rossin, Eur. J.

Inorg. Chem. (2017) 4909–4918. CSD codes: (a) ABAXIN, ABAXOT, ABAXUZ, ABAYAG, (b) FIKXII, (c) JEVCAP, (d) LENRIG, LENROM, (e) LUPKEN, (f) NETSUD, NETTAK.

[49] P. Li, X.-M. Yin, L.-L. Gao, S.-L. Yang, Q. Sui, T. Gong, E.-Q. Gao, ACS Appl. Nano Mater. 2 (2019) 4646–4654.